

Deep Learning for Improving Numerical Weather Prediction of Rainfall Extremes

Philipp Hess^{1,2}, Niklas Boers^{1,2,3}

¹Department of Mathematics and Computer Science, Freie Universität Berlin, Arnimallee 6, Berlin,
14195, Germany

²Potsdam Institute for Climate Impact Research (PIK), Telegraphenberg A31, Potsdam, 14473, Germany

³Department of Mathematics and Global Systems Institute, University of Exeter, Exeter, UK

Key Points:

- Correcting biases in the rainfall forecast of a numerical weather prediction ensemble with a deep neural network.
- Training with a weighted loss function enables the neural network to learn the heavy tailed target distribution.
- The method improves the relative frequency and categorical skill scores of rainfall extremes.

Corresponding author: Philipp Hess, hess@pik-potsdam.de

Abstract

The accurate prediction of rainfall, and in particular rainfall extremes, remains challenging for numerical weather prediction models. This can be attributed to subgrid-scale parameterizations of processes that play a crucial role in the multi-scale dynamics, as well as the strongly intermittent nature and the highly skewed, non-Gaussian distribution of rainfall. Here we show that a specific type of deep neural networks can learn rainfall extremes from a numerical weather prediction ensemble. A frequency-based weighting of the loss function is proposed to enable the learning of extreme values in the distributions' tails. We apply our framework in a post-processing step to correct for errors in the model-predicted rainfall. Our method yields a much more accurate representation of relative rainfall frequencies and improves the forecast skill of extremes by factors ranging from two to above six, depending on the event magnitude.

Plain Language Summary

Modelling rainfall is challenging because of its large variability in space and time, and its highly skewed distribution. Numerical weather prediction (NWP) models have to be simulated on discretized grids with finite resolution. Although important especially for the generation of rainfall, small-scale processes can therefore not be resolved explicitly and must be parameterized, i.e. included as empirical functions of the resolved variables. This introduces model biases that can lead to an underestimation of extreme events. Here we apply a deep neural network (DNN) to correct biases in the rainfall forecast of a NWP ensemble. The DNN is optimized with a loss function that includes weights to penalize rare extremes, and shows substantially improved performance in the prediction of extreme rainfall.

1 Introduction

Modelling and predicting rainfall, and in particular its extremes, is challenging because of the relevant multi-scale dynamics ranging from small-scale droplet interactions to large-scale weather systems, the high intermittency in space and time, as well the strongly non-Gaussian, right-skewed distribution (Koutsoyiannis, 2004b, 2004a). With larger spatial averages approximately following a positive trend expected from the thermodynamic Clausius-Clapeyron relation (Allan & Soden, 2008; Donat et al., 2013; Guerreiro et al., 2018), the frequency and severity of extreme rainfall are projected to increase in a warming atmosphere (Fischer & Knutti, 2016), making their accurate prediction even more challenging but also more important.

Numerical weather prediction (NWP) models, solving the fluid dynamical equations governing the dynamics of the atmosphere, are essential for weather forecasting, including the prediction of heavy rainfall events. Despite the large improvements made over the past decades (Bauer et al., 2015), considerable sources of error remain in the models, in particular for rainfall (Boyle & Klein, 2010). Global NWP models, with a resolution of about 20 km, cannot explicitly resolve many of the relevant small-scale processes. These processes need to be included as sub-grid parameterizations, i.e., they are written as empirical functions of the explicitly resolved (grid-scale) variables. These parameterizations of important processes involved in the generation of rainfall introduces biases and errors that can lead to an underestimation of extremes (Kang et al., 2015).

Recent work has shown promising results by including data-driven machine learning methods including neural networks (LeCun et al., 2015), into the traditional NWP workflow. Well-suited applications of neural networks range from data-assimilation (Bocquet et al., 2020), purely data-driven and hybrid weather prediction (Weyn et al., 2020; Rasp & Thuerey, 2021; Brenowitz & Bretherton, 2018; Watt-Meyer et al., 2021) to post-processing NWP output (Rasp & Lerch, 2018; Grönquist et al., 2021).

64 Here we apply a deep neural network (DNN) to correct the ECMWF (European
 65 Centre for Medium-Range Weather Forecasts, 2012) Integrated Forecast System (IFS)
 66 for biases by post-processing its rainfall output. When DNNs are tasked to infer a vari-
 67 able with large intermittency and a heavy-tailed distribution, such as rainfall, the op-
 68 timization with an averaging loss function such as the widely employed mean squared
 69 error (MSE) can be expected to lead to a good approximate of the distribution’s mean,
 70 but an underestimation of the extreme values in the tail. For rainfall, this problem has
 71 been addressed in different ways, e.g by translating the regression task into a classifica-
 72 tion problem (Agrawal et al., 2019; Sønderby et al., 2020), by using methods from com-
 73 puter vision (Tran & Song, 2019), and by employing a weighted loss function (Shi et al.,
 74 2017; Franch et al., 2020). The latter being composed of a weighted MSE and mean ab-
 75 solute error (MAE), with a set of five discrete weights determined by binned rainfall in-
 76 tensities. We show that a state-of-the-art DNN architecture is able to infer extreme val-
 77 ues in the far right tail of the target distribution from remotely sensed rainfall data us-
 78 ing a loss that combines a continuously weighted MSE with a structural similarity mea-
 79 sure. Notably, we use NWP ensemble simulations as input features, which do not exhibit
 80 an accurate representation of the extremes.

81 2 Materials and Methods

82 2.1 Integrated forecast system

83 Atmospheric variables simulated by an ensemble of the Integrated Forecast Sys-
 84 tem (IFS) from the European Center for Medium-Range Weather Forecasting (ECMWF)
 85 (European Centre for Medium-Range Weather Forecasts, 2012) are taken as inputs of
 86 the DNN. The ensemble consists of ten members with a spatial resolution of 0.5625° (or
 87 approximately 63 km) and 137 vertical levels. It is initialized twice daily at 06 and 18
 88 UTC with a 12 hour lead time and small perturbations in the initial conditions. In this
 89 work, the ensemble mean of the variables is used, which is provided at three-hourly time
 90 steps and 0.5° horizontal resolution.

91 2.2 Training data

92 The input features of the DNN are the three-hourly accumulated rainfall and verti-
 93 cal velocities of the IFS ensemble mean. The latter is taken from eleven pressure lev-
 94 els: 200, 250, 300, 400, 500, 600, 700, 800, 900, 950, and 1000 hPa. The vertical vel-
 95 ocity is dynamically linked to rainfall through convective processes and large-scale updrafts
 96 of warm, moist air (Pfahl et al., 2017; Müller et al., 2020). The satellite-based Tropical
 97 Rainfall Measurement Mission (TRMM) 3B42 V7 product (Huffman et al., 2007) is used
 98 as a training ground truth at three-hourly temporal resolution and is regridded to 0.5°
 99 by bilinear interpolation using the the Climate Data Operator (CDO) software (Schulzweida,
 100 2019), to match the IFS grid. The TRMM data is considered to have high accuracy espe-
 101 cially for heavy rainfall extremes (Boers et al., 2015). The geographic region of this
 102 study is the entire spatial coverage of the TRMM product, which ranges from 50° S to
 103 50° N and 180° W to 180° W. Further, the June, July and August season is used and
 104 split into a training set (1998-2008), a validation set (2009-2011) to optimize the hyper-
 105 parameters of the DNN model, and a test set for evaluation (2012-2014). Although the
 106 TRMM product is continued till present, a change of the satellites in 2014 has introduced
 107 significant biases, as shown in Figure S5, and the period after 2014 was therefore excluded.

108 2.3 Definition of rainfall extremes

109 We define extreme events as those 3-hourly time steps for which the rainfall sums
 110 exceed a pre-defined threshold. This threshold is determined individually for each grid

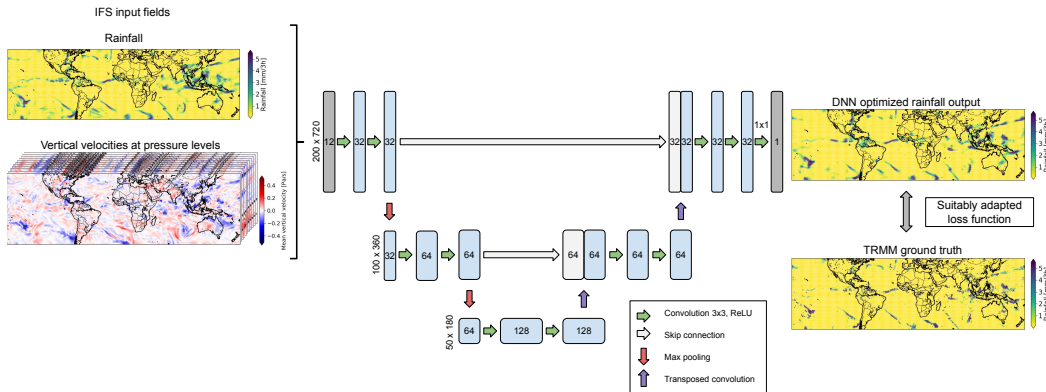


Figure 1. Sketch of the U-Net-based DNN architecture, the number of channels is indicated inside each layer. The horizontal dimensions per pooling level are given on the left.

111 cell in terms of percentiles, computed on the sets of 3-hourly time steps with rainfall amounts
 112 above 0.1 [mm/3h].

113 2.4 Neural network architecture

114 The DNN architecture is based on the U-Net (Ronneberger et al., 2015), a convo-
 115 lutional neural network that can capture multi-scale spatial patterns through a combi-
 116 nation of pooling operations for large-scale feature extraction and skip-connections to
 117 preserve small-scale, high-frequency information. The U-Net architecture has shown good
 118 performance in weather prediction and post-processing tasks (Grönquist et al., 2021; Weyn
 119 et al., 2020). The model, shown in Figure 1, takes the standardized spatial fields of the
 120 atmospheric variables as input, where the number of 12 input channels equals the number
 121 of variables times the corresponding number of pressure levels. The output layer has
 122 a single channel representing the rainfall rates and applies a rectified linear unit (ReLU)
 123 to ensure non-negative output values. The number of weights per layer is reduced by half
 124 compared to the original model from (Ronneberger et al., 2015), and only two max pool-
 125 ing operations are applied since a larger model size did not improve the performance.
 126 The ADAM optimizer (Kingma & Ba, 2017) was used for training the network together
 127 with a batch size of 64, a learning rate of 10^{-4} and early stopping to prevent overfitting.

128 2.5 Loss function

129 To improve the training regarding extreme values and the intermittency, we pro-
 130 pose the weighted loss function

$$L_{\lambda}(y, \hat{y}) = \frac{\lambda}{N} \sum_{i=1}^N w(y_i)(y_i - \hat{y}_i)^2 + (1 - \lambda)\text{MS-SSIM}(y, \hat{y}), \quad (1)$$

131 where N is the number of training examples, w is a weight function and y and \hat{y} are the
 132 target and prediction, respectively. The cost function is thus a convex sum of the weighted
 133 MSE and the so-called multi-scale structural similarity measure MS-SSIM (Wang et al.,

2003), introducing an additional hyperparameter λ . The MS-SSIM quantifies the structural similarity between two images. This is done through an iterative comparison of luminance, contrast and structure on different scales by downsampling and low-pass filtering the image signals (see supporting information). The weights w are defined as

$$w(y_i) = \min(\alpha e^{\beta y_i}, 1), \quad (2)$$

where α and β are hyperparameters. We optimize the hyperparameters on the validation set and set them to $\alpha = 0.007$, $\beta = 0.048$ and $\lambda = 0.158$. Since the relative frequency of 3-hourly rainfall events decreases approximately exponentially with increasing magnitude, the weights aim to account for the statistical imbalance. Ebert-Uphoff et al. (Ebert-Uphoff & Hilburn, 2020) also use an exponentially weighted MSE loss to emphasize rare and high values when training a DNN to estimate radar composite reflectivity from satellite imagery. In our case, we find that only optimizing with the weighted MSE leads to large biases which can be removed through the addition of the MS-SSIM into the loss. Further introducing bounds on the weights was crucial for a robust optimization of the network.

2.6 Baseline

A linear ridge regression (Hoerl & Kennard, 1970) with the IFS ensemble mean rainfall of a single grid-cell as input is used as a baseline model. Including the vertical velocity fields did not improve the performance of this baseline model.

3 Results

3.1 Evaluation of the continuous forecast skill of the deep learning model

We first compare the histograms of the relative frequencies of the 3-hourly rainfall values for the outputs from IFS, the different post-processing models, and the ground truth given by the TRMM remote sensing product (Figure 2a, 2b). The histograms of grid-cell values are computed over the entire part of the globe covered by the TRMM data (50°S to 50°N) and test set period. Training the DNN with an MSE or a MS-SSIM loss leads to a similar rainfall frequency distribution as the IFS ensemble mean and the linear ridge regression baseline, with over-representation of low rainfall frequencies and underestimation of the tail, as compared to the observational TRMM target. Training with the CW loss function in Eq. (1), instead, enables the DNN to infer a distribution that is substantially closer to the target distribution. The frequencies of low rainfall rates are correctly reduced, while at the same time achieving a better statistical representation of the extremes in the tail. The ridge regression shows the largest bias towards low rainfall rates, hence not improving the IFS output at all.

We assess the continuous forecast skill of the different models by computing the root mean square error (RMSE), mean error (ME) and the complex-wavelet structural similarity index (CW-SSIM) (Sampat et al., 2009) (see supporting information). The CW-SSIM allows a structural comparison of two images that is insensitive to small non-structural transformations such as rotation and translation, but sensitive to structural changes such as sharpness. Time steps with rainfall below a threshold of 0.1 [mm/3h] have been excluded before applying the error metrics since rainfall on such low scales cannot be measured accurately by satellite-based remote sensing (Huffman et al., 2007). The results are summarized in Table 1 as averages of the absolute cell-wise metrics. Training the DNN with the MS-SSIM leads to the lowest RMSE, while the CW loss function shows a ME similar to the MS-SSIM, and the highest structural similarity. Processing the IFS output with the ridge regression does not lead to improvements. Omitting rainfall from the input features and thus purely focusing on the vertical wind velocities W is not significantly affecting the performance of the model. The weighted loss function combined with

Table 1. Continuous validation statistics are given for the IFS ensemble mean, ridge regression and the DNNs trained with different loss functions and the input variables rainfall (P) and vertical velocity (W) from the IFS.

Model	Loss	Input	RMSE	%	ME	%	CW-SSIM	%
IFS	-	-	1.457	-	0.175	-	0.359	-
Ridge Regr.	MSE	P	1.473	-1.1	0.209	-19.4	0.359	0
DNN	MSE	W	1.375	5.6	0.165	5.7	0.388	8.1
DNN	MSE	P, W	1.372	5.8	0.166	5.1	0.395	10
DNN	MS-SSIM	P, W	1.368	6.1	0.136	22.3	0.441	22.8
DNN	CW	P, W	1.439	1.2	0.135	22.9	0.545	51.8

181 the MS-SSIM leads to an improvement of the ME by almost 23% and an improvement
 182 of the CW-SSIM metric by more than 50%.

183 3.2 Evaluation of the forecast skill of the deep learning model for ex- 184 tremes events

185 To evaluate the forecast skill for extreme events, categorical statistics can be com-
 186 puted from the contingency table containing the true positives and negatives, as well as
 187 the false positives and negatives (Table S1). A detailed definition of the events and skill
 188 scores is given in the supporting information. Table 2 summarizes the skill scores for events
 189 above the 95th percentile. The Heidke Skill Score (HSS), which is equal to zero for a ran-
 190 dom forecast and equal to one for a perfect forecast, is shown in Figure 2c for thresh-
 191 olds ranging from the 75th to the 99th percentile; corresponding results for the other scores
 192 are given in the supplementary Figures S1 to S4. The DNNs improve the scores com-
 193 pared to the IFS mean and ridge regression, in particular for events above the 90th and
 194 higher percentiles (Figure 2c). The DNN trained using the MS-SSIM alone as loss shows
 195 the highest scores below the 95th threshold. The proposed CW loss leads to significant
 196 improvements even above the 95th percentile (improving the IFS forecast by 192% in
 197 terms of the HSS) and yields the only skilful forecast for events above the 99th percentile
 198 (improving the IFS forecast by more than 500% in terms of the HSS). Note that the FAR
 199 score is not as strongly improved as the other skills, indicating slightly more frequent false
 200 alarms when optimizing with the CW loss. We attribute this to the highly localized, in-
 201 termittent nature of rainfall extremes and emphasize that - in view of the results for the
 202 other error metrics - the increased number of false positives is more than balanced by
 203 the increased number of true positives. The DNN trained with the combined weight (CW)
 204 introduced above leads to substantial improvements also for the spatial patterns of ex-
 205 tremes, in particular for regions with stronger extreme rainfall events (Figure 3).

206 4 Discussion

207 We introduced a DNN to model rainfall extremes from short-range numerical weather
 208 ensemble forecasts. To address the strong statistical imbalance of the training data, a
 209 loss function is introduced that combines a weighted MSE with a structural similarity
 210 measure. The proposed combined loss function (CW) is found to substantially improve
 211 the training with respect to extremes compared to using the MSE and MS-SSIM indi-
 212 vidually, which are two commonly used loss functions. For comparison, we show that post-
 213 processing the IFS mean with a ridge regression model does not lead to any improve-
 214 ments. This motivates the importance of a non-linear DNN architecture such as the U-

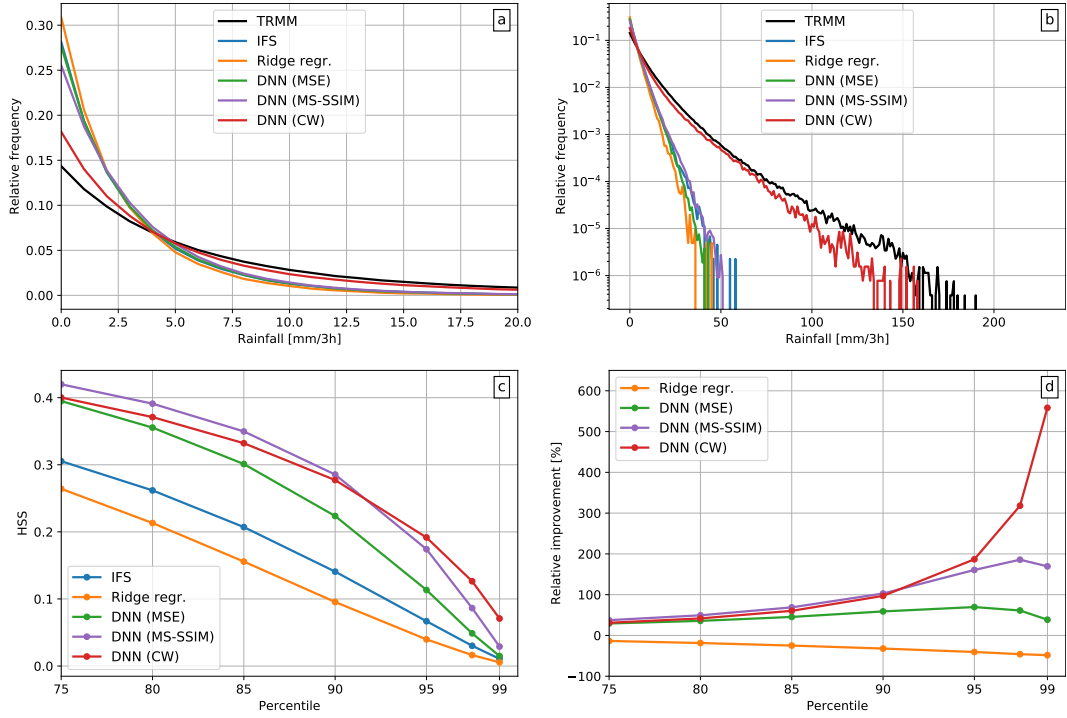


Figure 2. Relative rainfall frequencies and categorical extreme rainfall forecast scores for the different post-processing models compared to the IFS. Histograms of three-hourly rainfall event magnitudes are shown on a linear y-axis (a) and a logarithmic y-axis (b) for TRMM (black), IFS (blue), ridge regression (orange), DNN trained with the MSE loss (green), the MS-SSIM loss (purple) and the CW loss (red). (c) The Heidke Skill Score (HSS) for events above increasing percentile thresholds is shown for the IFS (blue), ridge regression (orange), DNN trained with the MSE loss (green), the MS-SSIM loss (purple), and with the CW loss proposed here (red). A HSS greater than zero implies an improvement over a random forecast, and HSS = 1 would imply a perfect forecast (see supporting information). (d) The relative improvement of the different machine learning methods over the IFS mean, in percentages.

Table 2. Event-based forecast skill scores for rainfall events above the 95th percentile. The percentage columns give the relative improvement over the IFS mean for each error metric and skill score.

Model	Loss	HSS	%	F1	%	CSI	%	POD	%	FAR	%
IFS	-	0.067	-	0.069	-	0.036	-	0.041	-	0.778	-
Ridge Regr.	MSE	0.040	-40	0.041	-41	0.021	-42	0.022	-46	0.775	0
DNN	MSE	0.113	69	0.115	67	0.061	69	0.066	61	0.567	27
DNN	MS-SSIM	0.174	160	0.177	157	0.097	169	0.115	180	0.622	20
DNN	CW	0.192	187	0.195	183	0.108	200	0.139	239	0.673	13

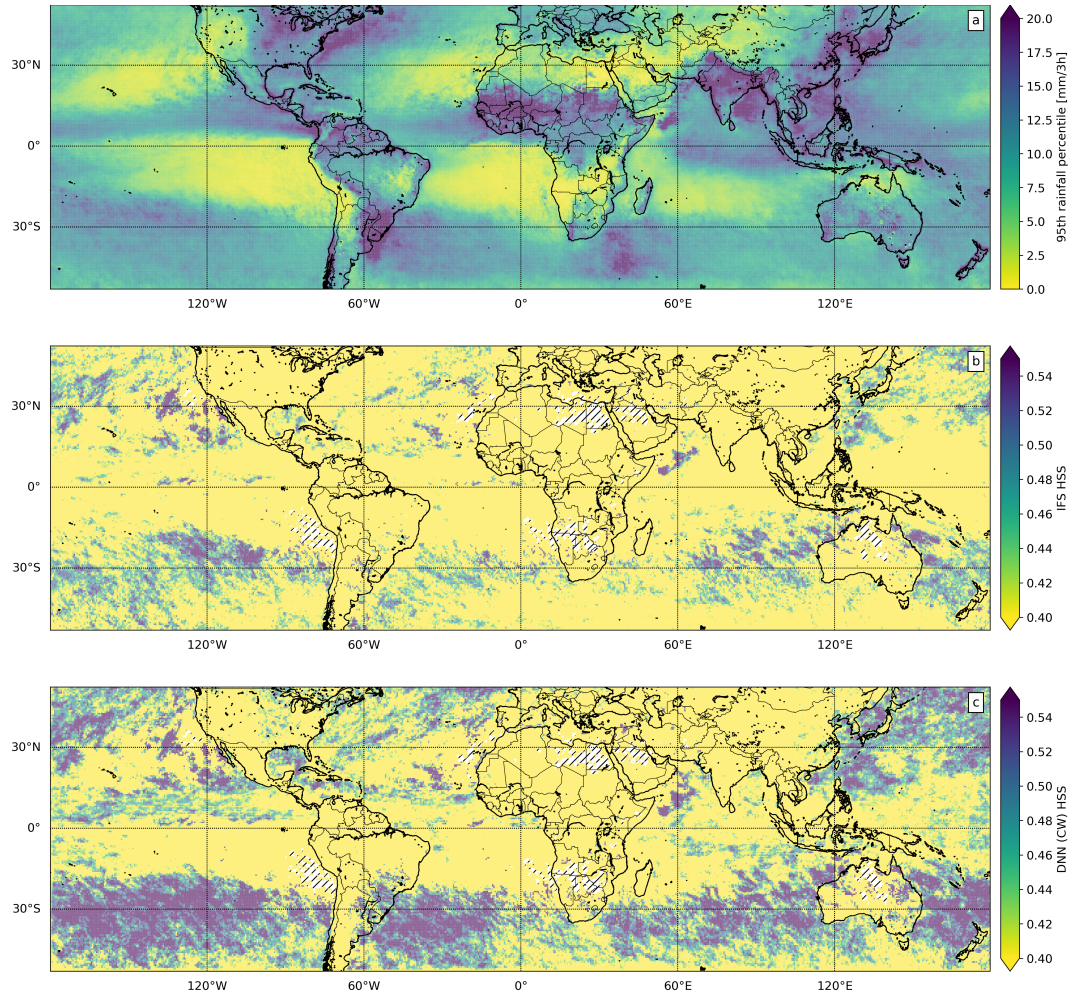


Figure 3. Spatial distribution of the 95th rainfall percentile and HSS for events above the 95th percentile. (a) The 95th percentile of the rainfall distribution at each grid cell of the TRMM dataset. (b) The spatially resolved HSS for the IFS mean. (c) The spatially resolved HSS for the DNN post-processed forecast, trained with the proposed CW loss. Hatched areas indicate grid-cells where the HSS could not be evaluated because no extreme events occurred in these locations.

215 Net. Moreover, our results suggest that the U-Net architecture is indeed capable of cap-
 216 turing the multi-scale spatial structure of rainfall accurately.

217 The CW loss substantially improves relative rainfall frequencies in the DNN out-
 218 put, the mean error and structural similarity of overall rainfall fields, as well as categor-
 219 ical skill scores for extreme events above the 90th and higher percentile, with strongly
 220 increasing rate of improvement for higher thresholds.

221 Taking the mean of the IFS ensemble is expected to damp the extremes in the fore-
 222 cast. Hence, the results of the IFS shown here do not represent the skill of single ensem-
 223 ble members to forecast extremes. Nevertheless, our results demonstrate the ability of
 224 the proposed DNN architecture to learn extremes that are not resolved in the input fea-
 225 tures, and to substantially improve their prediction.

226 Interestingly, the error statistics did not change significantly when rainfall was ex-
 227 cluded and only the vertical wind speed were considered as input features. This indicates
 228 that the DNN can learn a good representation of rainfall and especially its extremes from
 229 the vertical velocity alone.

230 Similarly surprising is the improved structural similarity when using the CW loss,
 231 compared to using the MS-SSIM alone as loss function. Although the considered fore-
 232 cast has a high temporal resolution of three hours, the forecast lead time of up to twelve
 233 hours is still comparably short. With applications to disaster prevention in mind, an ex-
 234 tension of the study to longer forecast lead times will be an important direction for fu-
 235 ture research. Further, making use of the entire IFS ensemble will allow to incorporate
 236 uncertainties into the framework that are essential for operational forecasting of extreme
 237 events.

238 Acknowledgments

239 The authors acknowledge funding by the Volkswagen Foundation, as well as the Euro-
 240 pean Regional Development Fund (ERDF), the German Federal Ministry of Education
 241 and Research and the Land Brandenburg for supporting this project by providing re-
 242 sources on the high performance computer system at the Potsdam Institute for Climate
 243 Impact Research. The Pytorch 1.7.0 (Paszke et al., 2019) source code for training and
 244 data processing is available at [github-link when accepted]. The IFS training data is avail-
 245 able for download at the Copernicus Climate Change Service (C3S) (Hersbach et al., 2020)
 246 ([https://cds.climate.copernicus.eu/cdsapp#!/dataset/reanalysis-era5-pressure](https://cds.climate.copernicus.eu/cdsapp#!/dataset/reanalysis-era5-pressure-levels)
 247 [-levels](https://cds.climate.copernicus.eu/cdsapp#!/dataset/reanalysis-era5-pressure-levels)). The TRMM (TMPA) data can be obtained at the Goddard Earth Sciences
 248 Data and Information Services Center (GES DISC) (Leptoukh, 2005) ([https://disc](https://disc.gsfc.nasa.gov/datasets/TRMM_3B42_7/summary)
 249 [.gsfc.nasa.gov/datasets/TRMM_3B42_7/summary](https://disc.gsfc.nasa.gov/datasets/TRMM_3B42_7/summary)).

250 References

- 251 Agrawal, S., Barrington, L., Bromberg, C., Burge, J., Gazen, C., & Hickey, J.
 252 (2019). *Machine learning for precipitation nowcasting from radar images*.
 253 Allan, R. P., & Soden, B. J. (2008). Atmospheric warming and the amplification of
 254 precipitation extremes. *Science*, *321*(5895), 1481–1484.
 255 Bauer, P., Thorpe, A., & Brunet, G. (2015). The quiet revolution of numerical
 256 weather prediction. *Nature*, *525*(7567), 47–55.
 257 Bocquet, M., Farchi, A., & Malartic, Q. (2020). Online learning of both state and
 258 dynamics using ensemble kalman filters. *Foundations of Data Science*, *0*(0), 0.
 259 Retrieved from <http://dx.doi.org/10.3934/fods.2020015> doi: 10.3934/
 260 fods.2020015
 261 Boers, N., Bookhagen, B., Marengo, J., Marwan, N., von Storch, J.-S., & Kurths,
 262 J. (2015). Extreme rainfall of the south american monsoon system: a dataset
 263 comparison using complex networks. *Journal of Climate*, *28*(3), 1031–1056.

- 264 Boyle, J., & Klein, S. A. (2010). Impact of horizontal resolution on climate model
 265 forecasts of tropical precipitation and diabatic heating for the twp-ice period.
 266 *Journal of Geophysical Research: Atmospheres*, *115*(D23).
- 267 Brenowitz, N. D., & Bretherton, C. S. (2018). Prognostic validation of a neural net-
 268 work unified physics parameterization. *Geophysical Research Letters*, *45*(12),
 269 6289–6298.
- 270 Donat, M., Alexander, L., Yang, H., Durre, I., Vose, R., Dunn, R., . . . others (2013).
 271 Updated analyses of temperature and precipitation extreme indices since the
 272 beginning of the twentieth century: The hadex2 dataset. *Journal of Geophysi-
 273 cal Research: Atmospheres*, *118*(5), 2098–2118.
- 274 Ebert-Uphoff, I., & Hilburn, K. (2020). Evaluation, tuning, and interpretation of
 275 neural networks for working with images in meteorological applications. *Bul-
 276 letin of the American Meteorological Society*, *101*(12), E2149–E2170.
- 277 European Centre for Medium-Range Weather Forecasts.
 278 (2012). *The ECMWF ensemble prediction system*.
 279 https://www.ecmwf.int/sites/default/files/the_ECMWF_Ensemble_prediction_system.pdf.
- 280
- 281 Fischer, E. M., & Knutti, R. (2016). Observed heavy precipitation increase confirms
 282 theory and early models. *Nature Climate Change*, *6*(11), 986–991.
- 283 Franch, G., Nerini, D., Pendesini, M., Coviello, L., Jurman, G., & Furlanello, C.
 284 (2020). Precipitation nowcasting with orographic enhanced stacked general-
 285 ization: Improving deep learning predictions on extreme events. *Atmosphere*,
 286 *11*(3), 267.
- 287 Grönquist, P., Yao, C., Ben-Nun, T., Dryden, N., Dueben, P., Li, S., & Hoefler,
 288 T. (2021). Deep learning for post-processing ensemble weather forecasts.
 289 *Philosophical Transactions of the Royal Society A*, *379*(2194), 20200092.
- 290 Guerreiro, S. B., Fowler, H. J., Barbero, R., Westra, S., Lenderink, G., Blenkinsop,
 291 S., . . . Li, X.-F. (2018). Detection of continental-scale intensification of hourly
 292 rainfall extremes. *Nature Climate Change*, *8*(9), 803–807.
- 293 Hersbach, H., Bell, B., Berrisford, P., Hirahara, S., Horányi, A., Muñoz-Sabater, J.,
 294 . . . others (2020). The era5 global reanalysis. *Quarterly Journal of the Royal
 295 Meteorological Society*.
- 296 Hoerl, A. E., & Kennard, R. W. (1970). Ridge regression: Biased estimation for
 297 nonorthogonal problems. *Technometrics*, *12*(1), 55–67.
- 298 Huffman, G. J., Bolvin, D. T., Nelkin, E. J., Wolff, D. B., Adler, R. F., Gu, G., . . .
 299 Stocker, E. F. (2007). The trmm multisatellite precipitation analysis (tmpa):
 300 Quasi-global, multiyear, combined-sensor precipitation estimates at fine scales.
 301 *Journal of hydrometeorology*, *8*(1), 38–55.
- 302 Kang, I.-S., Yang, Y.-M., & Tao, W.-K. (2015). Gcms with implicit and explicit
 303 representation of cloud microphysics for simulation of extreme precipitation
 304 frequency. *Climate Dynamics*, *45*(1-2), 325–335.
- 305 Kingma, D. P., & Ba, J. (2017). *Adam: A method for stochastic optimization*.
- 306 Koutsoyiannis, D. (2004a, aug). Statistics of extremes and estimation of extreme
 307 rainfall: II. Empirical investigation of long rainfall records. *Hydrological Sci-
 308 ences Journal*, *49*(4), 591–610. doi: 10.1623/hysj.49.4.591.54424
- 309 Koutsoyiannis, D. (2004b, aug). Statistics of extremes and estimation of extreme
 310 rainfall: I. Theoretical investigation. *Hydrological Sciences Journal*, *49*(4),
 311 575–590. doi: 10.1623/hysj.49.4.575.54430
- 312 LeCun, Y., Bengio, Y., & Hinton, G. (2015). Deep learning. *nature*, *521*(7553), 436–
 313 444.
- 314 Leptoukh, G. (2005). Nasa remote sensing data in earth sciences: Processing, archiv-
 315 ing, distribution, applications at the ges disc. In *Proc. of the 31st intl symposi-
 316 um of remote sensing of environment*.
- 317 Müller, A., Niedrich, B., & Névir, P. (2020). Three-dimensional potential vortic-
 318 ity structures for extreme precipitation events on the convective scale. *Tellus*

- 319 *A: Dynamic Meteorology and Oceanography*, 72(1), 1–20.
- 320 Paszke, A., Gross, S., Massa, F., Lerer, A., Bradbury, J., Chanan, G., . . . Chintala,
321 S. (2019). Pytorch: An imperative style, high-performance deep learning li-
322 brary. In H. Wallach, H. Larochelle, A. Beygelzimer, F. d'Alché-Buc, E. Fox, &
323 R. Garnett (Eds.), *Advances in neural information processing systems 32* (pp.
324 8024–8035). Curran Associates, Inc.
- 325 Pfahl, S., O’Gorman, P. A., & Fischer, E. M. (2017). Understanding the regional
326 pattern of projected future changes in extreme precipitation. *Nature Climate*
327 *Change*, 7(6), 423–427.
- 328 Rasp, S., & Lerch, S. (2018). Neural networks for postprocessing ensemble weather
329 forecasts. *Monthly Weather Review*, 146(11), 3885–3900.
- 330 Rasp, S., & Thuerey, N. (2021). Data-driven medium-range weather prediction with
331 a resnet pretrained on climate simulations: A new model for weatherbench.
332 *Journal of Advances in Modeling Earth Systems*, 13(2), e2020MS002405.
- 333 Ronneberger, O., Fischer, P., & Brox, T. (2015). U-net: Convolutional networks for
334 biomedical image segmentation. In *International conference on medical image*
335 *computing and computer-assisted intervention* (pp. 234–241).
- 336 Sampat, M. P., Wang, Z., Gupta, S., Bovik, A. C., & Markey, M. K. (2009). Com-
337 plex wavelet structural similarity: A new image similarity index. *IEEE trans-*
338 *actions on image processing*, 18(11), 2385–2401.
- 339 Schulzweida, U. (2019, October). *Cdo user guide*. Retrieved from [https://doi.org/](https://doi.org/10.5281/zenodo.3539275)
340 [10.5281/zenodo.3539275](https://doi.org/10.5281/zenodo.3539275) doi: 10.5281/zenodo.3539275
- 341 Shi, X., Gao, Z., Lausen, L., Wang, H., Yeung, D.-Y., kin Wong, W., & chun Woo,
342 W. (2017). *Deep learning for precipitation nowcasting: A benchmark and a*
343 *new model*.
- 344 Sønderby, C. K., Espeholt, L., Heek, J., Dehghani, M., Oliver, A., Salimans, T., . . .
345 Kalchbrenner, N. (2020). *Metnet: A neural weather model for precipitation*
346 *forecasting*.
- 347 Tran, Q.-K., & Song, S.-k. (2019). Computer vision in precipitation nowcasting: Ap-
348 plying image quality assessment metrics for training deep neural networks. *At-*
349 *mosphere*, 10(5), 244.
- 350 Wang, Z., Simoncelli, E. P., & Bovik, A. C. (2003). Multiscale structural similarity
351 for image quality assessment. In *The thirty-seventh asilomar conference on sig-*
352 *nals, systems & computers, 2003* (Vol. 2, pp. 1398–1402).
- 353 Watt-Meyer, O., Brenowitz, N. D., Clark, S. K., Henn, B., Kwa, A., McGibbon,
354 J. J., . . . Bretherton, C. S. (2021). *Correcting weather and climate models by*
355 *machine learning nudged historical simulations*.
- 356 Weyn, J. A., Durran, D. R., & Caruana, R. (2020). Improving data-driven
357 global weather prediction using deep convolutional neural networks on a
358 cubed sphere. *Journal of Advances in Modeling Earth Systems*, 12(9),
359 e2020MS002109.